Geophys. J. Int. (2005) **162,** 927–934 doi: 10.1111/j.1365-246X.2005.02699.x

Scattering of elastic waves by a 2-D crack using the Indirect Boundary Element Method (IBEM)

Ursula Iturrarán-Viveros,[1] Rossana Vai[1] and Francisco J. Sánchez-Sesma[2]

[1] *Instituto Mexicano del Petróleo; Eje Central Lázaro Cárdenas* 152*, C.P.* 07730*, México D.F., México. E-mails: uiturrar@imp.mx; rvai@imp.mx*
[2] *Instituto de Ingeniería, UNAM; Cd. Universitaria, Apdo. Postal* 70-472*; C.P.* 04510*; México D.F., México. E-mail: sesma@servidor.unam.mx*

Accepted 2005 May 24. Received 2005 May 19; in original form 2004 June 13

SUMMARY

The scattering of elastic waves by cracks is an old problem and various ways to solve it have been proposed in the last decades. One approach is using dual integral equations, another useful and common formulation is the Boundary Element Method (BEM). With the last one, the boundary conditions of the crack lead to hyper-singularities and particular care should be taken to regularize and solve the resulting integral equations.

In this work, instead, the Indirect Boundary Element Method (IBEM) is applied to study problems of zero-thickness 2-D cracks. The IBEM yields the Crack Opening Displacement (COD) which is used to evaluate the solution away from the crack. We use a multiregional approach which consists of splitting a boundary S into two identical boundaries S^+ and S^- chosen such that the cracks lie in the interface. The resulting integral equations are not hyper-singular and wave propagation within media that contain zero-thickness cracks can be rigorously solved.

In order to validate the method, we deal with the scalar case, namely the scattering of antiplane *SH* waves by a 2-D crack. We compare results against a recently published analytic solution, obtaining an excellent agreement. This comparison gives us confidence to study cases where no analytic solutions exist. Some examples of incidence of *P*- or *SV* waves are depicted and the salient aspects of the method are also discussed.

Key words: boundary element method, cracks, diffraction, scattering, wave propagation.

1 INTRODUCTION

The scattering and diffraction of elastic waves by cracks or inclusions is an important engineering problem and has been investigated by numerous authors. From the physical point of view the question that arises is up to what degree a local perturbation in a medium modifies the scattered wavefield. For instance, in seismic monitoring, to enhance oil recovery a crucial problem is to determine zones where there are changes in the physical properties. In naturally fractured reservoirs these changes can sometimes be explained by the extensive presence of empty or fluid-filled cracks and cavities. These heterogeneities determine the pathways and volume of crustal fluid movements and can drastically change productivity in oil fields. Using statistical hypothesis or equivalent media theories, diffraction patterns caused by many cracks can be deduced from that of a single crack (see Hudson 1986).

The problem of scattering from a finite crack is an old one, hence the existing literature on the subject is vast. For instance, Ang & Knopoff (1964a,b), dealt with diffraction of elastic waves by solving a system of integral equations. Mal (1970) studied the problem of interaction of elastic waves with a Griffith crack by solving a Fredholm integral equation of the second kind to determine the diffracted field. From the integral equation an asymptotic development of the solution is obtained valid for wavelengths longer than the length of the crack. From the point of view of ray theory Achenbach *et al.* (1982) gathered a complete study. Coutant (1989) used a boundary integral equation method (considering interior and exterior regions), combined with the discrete wavenumber representation, to study one or several fluid-filled cracks. van der Hijden & Neerhof (1984) study scattering of *P–SV* waves by a 2-D crack. They use an integral equation formulation to deal with the jump in the particle displacement across the crack. Then solve the resulting integral equation using a complete sequence of Chebyshev polynomials. A study of the influence of the crack geometry on Rayleigh wave propagation is carried out using the IBEM by Hevin *et al.* (1998). In order to analyse seismic response caused by hydraulic fractures Pointer *et al.* (1998) used the IBEM to show that diffraction from crack tips can, in principle, be used to locate and to determine the hydro-fracture size. Another approach, within the Boundary Element Methods (BEMs) is the one given by Prosper (1998) where the author develops a new tool: the Traction Boundary Element Method (TBEM) to model scattering of waves by cracks in elastic media. Just as for the traditional formulation, a critical step in the TBEM is the evaluation of integrals with hyper-singular kernels.

When dealing with the problem of scattering of elastic waves by cracks using the BEM, the boundary conditions of the crack lead

to hyper-singular formulations and particular care should be taken to regularize and solve the resulting integral equations, (see e.g. Bonnet 1995). The aim of this paper is to overcome the problem of singularities and to validate the IBEM to solve problems related to diffraction of plane waves in a medium with cracks. To this end we compare the solution obtained using the IBEM with an analytic solution by Sánchez-Sesma & Iturrarán-Viveros (2001) for the *SH* case of a zero-thickness finite crack embedded in a 2-D elastic isotropic homogeneous space. The validation of the IBEM for this problem enables us to use it confidently to solve problems where there are not known analytic solutions.

In the next section we proceed with the formulation of the problem. We explain how the multiregional approach can lead to a single-layer integral representation and no hyper-singularities arise. The multiregional approach is somewhat different to the one that Bonnet (1995) uses. Therefore, numerical instability related to the interior problem, if any, is avoided. In our formulation the domain in which we can obtain cheap, stable and accurate results is limited, but we can easily extend it by means of the Somigliana representation theorem (see for instance Achenbach 1973; Aki & Richards 1980; Banerjee & Butterfield 1981). Finally, in the last section we show and discuss some new numerical results in both time and frequency domains. The issues discussed herein have their natural counterparts in 3-D problems which are studied elsewhere.

2 FORMULATION OF THE PROBLEM

A crack can be thought of as the limiting case of a flat cavity as its thickness goes to zero. As discussed by Cruse (1988), the conventional BEM degenerates for the flat crack and is no longer a valid numerical modelling tool. The degeneracy is essentially associated with the ill-posed nature of problems with two co-planar surfaces. In addition BEMs suffer from numerical noise due to characteristic frequencies associated to closed areas or volumes. These problems can be overcome when using a multiregional approach.

Consider propagation of elastic waves in an elastic homogeneous isotropic 2-D medium, the displacement **u** will be a function of the position inside the plane. If the reference system is taken such that the *y*-axis is perpendicular to the *xz*-plane we can write the displacement as a function of the two coordinate system variables, that is $\mathbf{u} = \mathbf{u}(x, z)$. Under these hypothesis Navier's equations simplify by decoupling motion out-of-plane (u_y) and in-plane (u_x and u_z). The displacement out of the *xz*-plane is solution of a scalar equation and this case is known as the *SH*-wave propagation, whereas the displacement within the *xz*-plane is the solution of two coupled equations which describe the coupled *P*- and *SV* waves. The second-degree partial differential equations are in terms of the unknown displacements and of the elastic parameters of the medium (typically we use the Lame's constants λ and μ). The shear waves *SH* and *SV* are transversely polarized waves with propagation speed $\beta = \sqrt{\mu/\rho}$ (being ρ the density). Compression *P* waves are longitudinally polarized waves travelling at speed $\alpha = \sqrt{(\lambda + 2\mu)/\rho}$.

Since linearity holds, the total displacement field can be expressed as superposition of an incident or reference field, plus a diffracted field, that is,

$$\mathbf{u} = \mathbf{u}^{(0)} + \mathbf{u}^{(d)} \; ; \tag{1}$$

where the superscripts (0) and (*d*) represent the reference and diffracted fields, respectively. The incident field is analytically known and for a harmonic plane wave as the one in Fig. 1 we write

$$\mathbf{u}^{(0)} = \mathbf{u}_0(\omega) \exp\left(ikx \sin\gamma - ikz \cos\gamma\right) \tag{2}$$

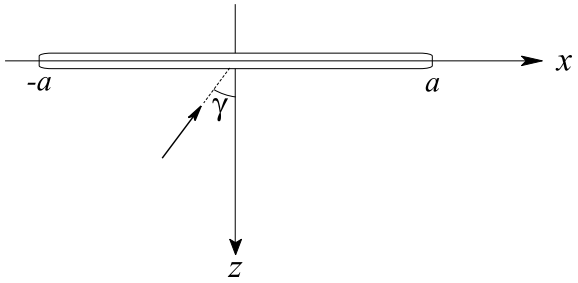

Figure 1. The *x*-axis of the reference system is taken perpendicular to the 2-D domain determined by the *xz*-plane. The incident plane wave is indicated by the ray and it comes from infinite positive *z*. Where γ is the incidence angle between the ray path and the *z*-axis (positive taken clockwise). We consider *SH*- and *P–SV* incident waves.

where $\mathbf{u}_0(\omega)$ is the wave amplitude, ω is the angular frequency, k is the wavenumber ($k = \omega/c$), c is the propagation velocity (α or β), and γ is the incidence angle. The time dependence of **u**, that is, $\exp(-i\omega t)$, is omitted here and hereafter. The diffracted field is unknown. Therefore, the goal is to find a suitable algorithm to compute it or to find **u** directly. BEMs have proved to be very useful to compute the displacement field in fractured media (Aliabadi 1997). In this paper we give an original formulation of the IBEM to compute the diffracted field. The basic idea is to manipulate the real boundary of a crack, introducing fictitious surfaces and partitioning the original domain. When compared with the traditional solution scheme, this strategy implies increased memory requirements, but with powerful benefits. For instance, we can rigorously solve zero-thickness cracks. An irregular 2-D zero-thickness crack can be thought of as an irregular segment (Fig. 2a). Firstly, let us draw a straight line passing by the extremities of the crack, (see Fig. 2b), and use it to extend the segment up to infinity (Fig. 2c). Of course, these auxiliary lines (2-D case) or surfaces (3-D case) are constructed finite and in practice can be relatively small. The smallest region we have used in the given examples for the crack's elongation is *a*, half the crack's size. Then the curve in which the crack is embedded is divided into two complementary 2-D subdomains, being S^+ and S^- their boundaries (Figs 2d and 2e).

The illuminated surface S^+ is the boundary which is first struck by the incident wave. The shaded surface is denoted by S^-. The physics of the problem is recovered by suitable boundary conditions along S^+ and S^-. Particularly, we need to set continuity of displacements and tractions on the crack's elongation and zero tractions on the contour of the crack. The multi-domain approach is not a new idea (Bonnet 1995) and we propose, instead, to split two infinite subdomains. This device will be very useful for the numerical method we planned to use; details will be discussed further.

Following Sánchez-Sesma & Campillo (1991) for each of the boundaries S^+ and S^-, the IBEM equations are

$$u^{(d)}(\mathbf{x}) = \int_S \phi(\xi) G(\mathbf{x}, \xi)\, dS_\xi \; , \tag{3}$$

$$t^{(d)}(\mathbf{x}) = \int_S \phi(\xi) T(\mathbf{x}, \xi)\, dS_\xi , \tag{4}$$

where with appropriate subindices (3) and (4) describe either *SH*- or *P–SV* wave propagation; $u^{(d)}$ ($t^{(d)}$) is the diffracted displacement (traction); $G(\mathbf{x}, \xi)(T(\mathbf{x}, \xi))$ is the displacement (traction) Green's function, i.e. the displacement (traction) at a point **x** caused by a unit force at a point ξ; $\phi(\xi)$ is the force density at ξ and S is the boundary. The integrals are computed along S. The expression of the

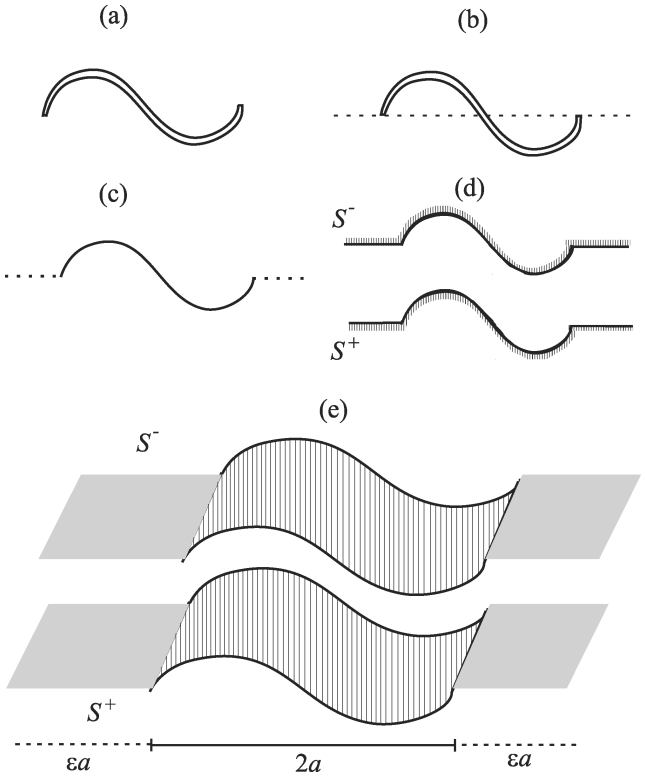

Figure 2. The profile of a crack (a) is extended tracing a straight line passing by the extremities of the fracture (b), so that the plane is divided into two subdomains (c). The two subdomains can be handled separately and their boundaries are named S^+ and S^- (d). (e) A 3-D view of what the procedure of splitting the two domains means. We consider the size of the crack as $2a$ and the extended non-physical domain discretized has size ϵa on each side of the crack.

Green's functions for the 2-D case can be found in Sánchez-Sesma & Campillo (1991).

Green's functions are singular for $x = \xi$, but they can be integrated using power series (for G) or analytically in the Cauchy principal value sense (for T). Moreover $G(\mathbf{x}, \xi)$ on S^+ is identical to $G(\mathbf{x}, \xi)$ on S^- since the two surfaces perfectly match. The same can be nearly stated for T when the unit normal vectors to S^+ and S^- are equal, the only difference being in the sign of the singular term.

Numerical realization of boundary conditions of continuity at a point $\mathbf{x}$ on the crack elongation are expressed by:

$$\sum_{i=1}^{N} \left[\phi^+(x_i) - \phi^-(x_i)\right] \int_{\Delta S_i} G(\mathbf{x}, \xi)\, dS_\xi = 0, \tag{5}$$

$$\frac{1}{2}\left[\phi^+(\mathbf{x}) + \phi^-(\mathbf{x})\right] + \sum_{i=1}^{N} \left[\phi^+(x_i) - \phi^-(x_i)\right] \int_{\Delta S_i} T(\mathbf{x}, \xi)\, dS_\xi = 0, \tag{6}$$

where the first equation corresponds to continuity of displacement and the second defines continuity of traction. The surface S, interface between the two subdomains, is discretized into straight segments ΔS_i, the length of which is chosen to be at least one-sixth of the wavelength for the frequency under study. The force density ϕ is considered to be constant along ΔS_i so that it is evaluated just at its middle point x_i. The integrals in eq. (5) are computed expanding G in power series when $\mathbf{x} \in \Delta S_i$. The integral in eq. (6) is null when $\mathbf{x} \in \Delta S_i$, since the singularity is explicitly solved and expressed by the first term of the equation. Numerical realization of boundary conditions at a point $\mathbf{x}$ on the crack is expressed by:

$$\frac{1}{2}\phi^+(\mathbf{x}) + \sum_{i=1}^{N} \phi^+(x_i) \int_{\Delta S_i} T(\mathbf{x}, \xi)\, dS_\xi = -t^{(0)+}(\mathbf{x})\,, \tag{7}$$

$$-\frac{1}{2}\phi^-(\mathbf{x}) + \sum_{i=1}^{N} \phi^-(x_i) \int_{\Delta S_i} T(\mathbf{x}, \xi)\, dS_\xi = -t^{(0)-}(\mathbf{x}). \tag{8}$$

Note that in eqs (5)–(8) subscripts for force density and Green's functions are omitted. In the *SH* case, we have $2N$ unknowns with $2(N - M)$ continuity and $2M$ crack conditions, where M is the number of segment used to discretize the crack. Following the same notation, in the *P–SV* problem, there are $4N$ unknowns with $4(N - M)$ continuity and $4M$ crack conditions.

Eqs (5)–(8) allow us to form a non-singular system for which there is a unique solution. Once the unknown force densities are found one can substitute them into eq. (3), properly discretized, to obtain the displacement at any point $\mathbf{x}$ of the medium. However, there is a better strategy we can adopt. Considering the whole 2-D space domain and recalling Somigliana's identity in the frequency domain, we can write the following integral equation

$$u^{(d)}(\xi) = \int_S \left[t^{(d)}(\mathbf{x})G(\mathbf{x}, \xi) - u^{(d)}(\mathbf{x})T(\mathbf{x}, \xi)\right] dS_\mathbf{x}, \tag{9}$$

where ξ lies inside one of the subdomains, $\mathbf{x} \in S$ and $S = S^+ \cup S^-$. It is convenient that normal vector points away from the physical domain (as for S^+). This means that the normal at S^- should change direction. In that case diffracted and Green's tractions satisfy

$$\begin{aligned} t_i^{(d)+}\big|_S &= -t_i^{(d)-}\big|_S \\ T^+(\mathbf{x}, \xi) &= -T^-(\mathbf{x}, \xi), \end{aligned} \tag{10}$$

Moreover, as the Green's functions $G(\mathbf{x}, \xi)$ are independent of the normal vector definition, eq. (9) can be rewritten as:

$$u^{(d)}(\xi) = \int_{S^+} \Delta u(\mathbf{x}) T^+(\mathbf{x}, \xi)\, dS_\mathbf{x}, \tag{11}$$

where T^+ is the traction Green's function calculated accordingly to the unit normal vector pointing outward the illuminated space, and $\Delta u(\mathbf{x}) = u^+(\mathbf{x}) - u^-(\mathbf{x})$ is the Crack Opening Displacment (COD) which is the displacement difference between the shaded and illuminated sides of the crack. Unnecessary operations are cleared away and accuracy increases by using eq. (11) instead of (9). In numerical applications there is an important benefit of the use of Somigliana's identity instead of the classical IBEM equations. S^+ and S^- should be infinite surfaces, but this is manifestly inconsistent with any numerical realization. The cutting of S is required at any effect. The numerical method we choose (the IBEM) can be seen as realization of Huygens' principle: wave fronts are reproduced by radiating sources distributed along a surface. When S is cut, the set of sources along this boundary is interrupted and artificial diffraction at the edges is introduced. This spurious effects are not visible inside suitable space-time windows, depending on the length of S, the location of the observer and on wave speeds. Displacement along the crack can be calculated considering a short extension of S but accurate computation of displacement at any point and time of the media, would require a very large extension of S and this is reflected in high computational costs. By introducing the extended non-physical regions (next to each of the crack's edges) we are adding extra unknowns to the system of linear equations to be solved. This is a current limitation of the method because it increases computational costs (specially for 3-D cases). We could alleviate the problem by using sparse matrix computations (see Ortiz-Alemán

et al. 1998). With the use of Somigliana's identity the IBEM is used to calculate the COD along the crack, so that numerical noise is easily avoided and we obtain clean solutions at any point or time with low computational costs.

3 NUMERICAL RESULTS

In this section, we show comparisons between the results obtained using the IBEM and results obtained with an analytic solution for a plane crack with zero thickness (see Sánchez-Sesma & Iturrarán-Viveros 2001 and the appendix for further details)

Synthetic seismograms are computed from frequency-domain results using a Fast Fourier Transform (FFT) algorithm. In Figs 3 and 4 we show synthetic seismograms for an incident *SH* plane wave with incidence angle $\gamma = 0^{\circ}(\gamma = 30^{\circ})$ impinging on the crack in Fig. 1. A Ricker wavelet with characteristic period $t_p = 1$ s centred at $t_s = 2$ s is chosen to excite the system. The analytical solution and the numerical (calculated using the IBEM) solutions are superimposed. Hereafter we refer to a dimension-less domain where the wave propagation velocity and the density are both a unit. In this example the finite crack is located within the interval $[-1, 1]$ along the x-axis. Fig. 3(a) shows that the diffracted wavefield reaches 11 equally spaced stations located at $z = 1$ with $x \in [-2, 2]$ (i.e. on the illuminated side of the crack). Fig. 3(b) shows the diffracted wavefield at 11 equally spaced stations located at $z = -1$ with $x \in [-2, 2]$. Energy spread to the shaded strip created by the crack and the wave front. Cylindrical diffracted waves are generated at the edges of the crack. The first pulse corresponds to the incident wave then we see the arrival of the reflected and diffracted waves. The agreement between the analytical and the IBEM solutions is very good for both incidences. Therefore, we can confidently apply the method to a problem where there is not known analytic solution. For example a zero-thickness, semi-circular crack (depicted in Fig. 5). In Fig. 6, an *SH* plane wave with incidence angle $\gamma = 30^{\circ}$ (with respect to the z-axis) strikes the semi-circular crack with radius $r = a = 1$ and zero thickness. In order to identify all the generated waves when an incident plane wave strikes the crack, in the snapshots we

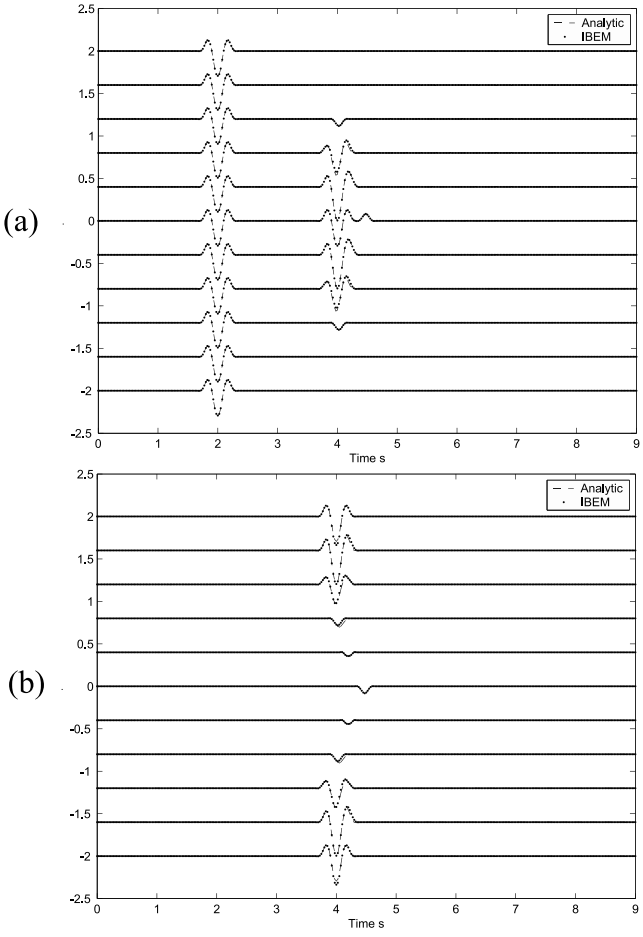

Figure 3. Seismograms for an incident wave front with incidence angle $\gamma = 0^{\circ}$. The incident time signal is a Ricker wavelet with characteristic period $t_p = 2.0$ s. The finite crack is located within the interval $[-1, 1]$. (a) Seismograms for a line of equally spaced receivers is located at $z = 1$. The incident wave front reaches stations on the illuminated side before than the crack. Therefore, the wave front does not have perturbations. After 2 s. the reflected and diffracted waves arrive. (b) Seismograms for a line equally spaced receivers located at $z = -1$. Since these stations are on the shaded side of the crack the incident wave front is perturbed.

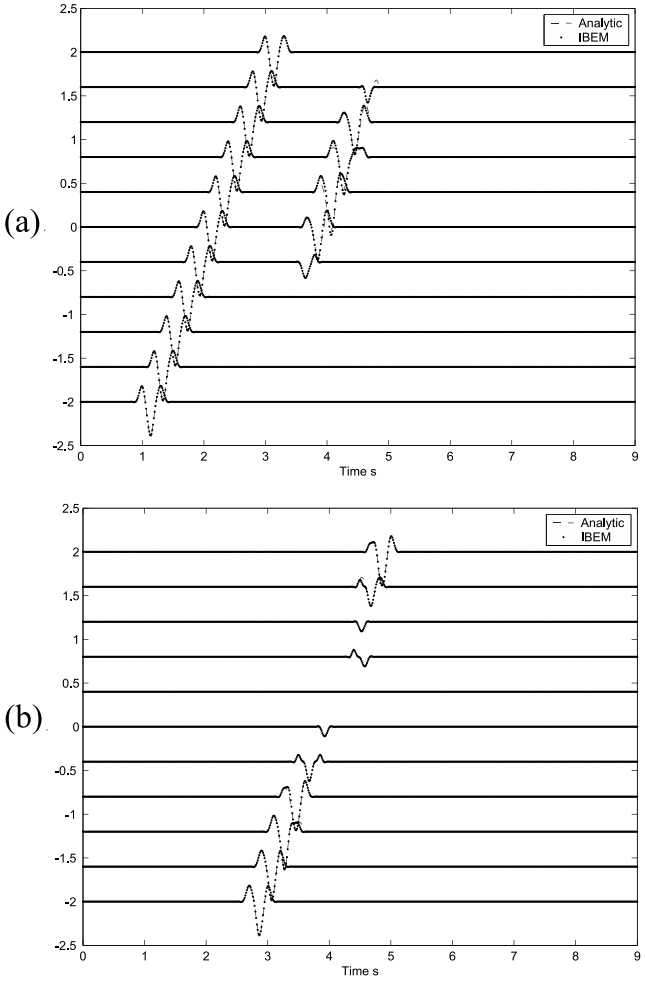

Figure 4. Seismograms for an incident wave front with incidence angle $\gamma = 30^{\circ}$. The incident time signal is a Ricker wavelet with characteristic period $t_p = 2.0$ s. The agreement between results obtained with the analytic solution and with the IBEM is excellent. The finite crack is located within the interval $[-1, 1]$. (a) Seismograms for a line of equally spaced receivers is located at $z = 1$. The incident wave front reaches stations on the illuminated side before than the crack. Therefore, the wave front does not have perturbations. After 3s the reflected and diffracted waves arrive. (b) Seismograms for a line equally spaced receivers located at $z = -1$ in the shaded region, energy is due to diffracted waves.

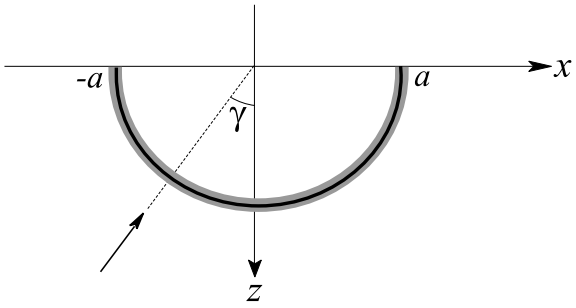

Figure 5. The x-axis of the reference system is taken perpendicular to the 2-D domain determined by the xz-plane. The incident plane wave is indicated by the ray and it comes from infinite positive z. Where γ is the incidence angle between the ray path and the z-axis (positive taken clockwise). We consider *SH*- and *P–SV* incident waves striking a semi-circular crack.

have labelled different waves with different numbers. The incident time signal is a Ricker wavelet with characteristic period $t_p = 1.0$ s. We are able to identify the following:

(1) the incident wave,
(2) the reflected wave,
(3) the first cylindrical diffracted wave generated at the left edge of the crack on the shaded side,
(4) the first diffracted wave generated at the left edge of the crack on the illuminated side and
(5) the first diffracted wave generated at the right edge of the crack.

For the *P–SV* case we consider a finite straight crack located within the interval $[-1, 1]$. Contour maps of displacement amplitudes for 41 equally spaced receivers located at $z = -0.1$ with $x \in [-2, 2]$ against the normalized frequency $\eta = \omega a/\pi\beta$ are

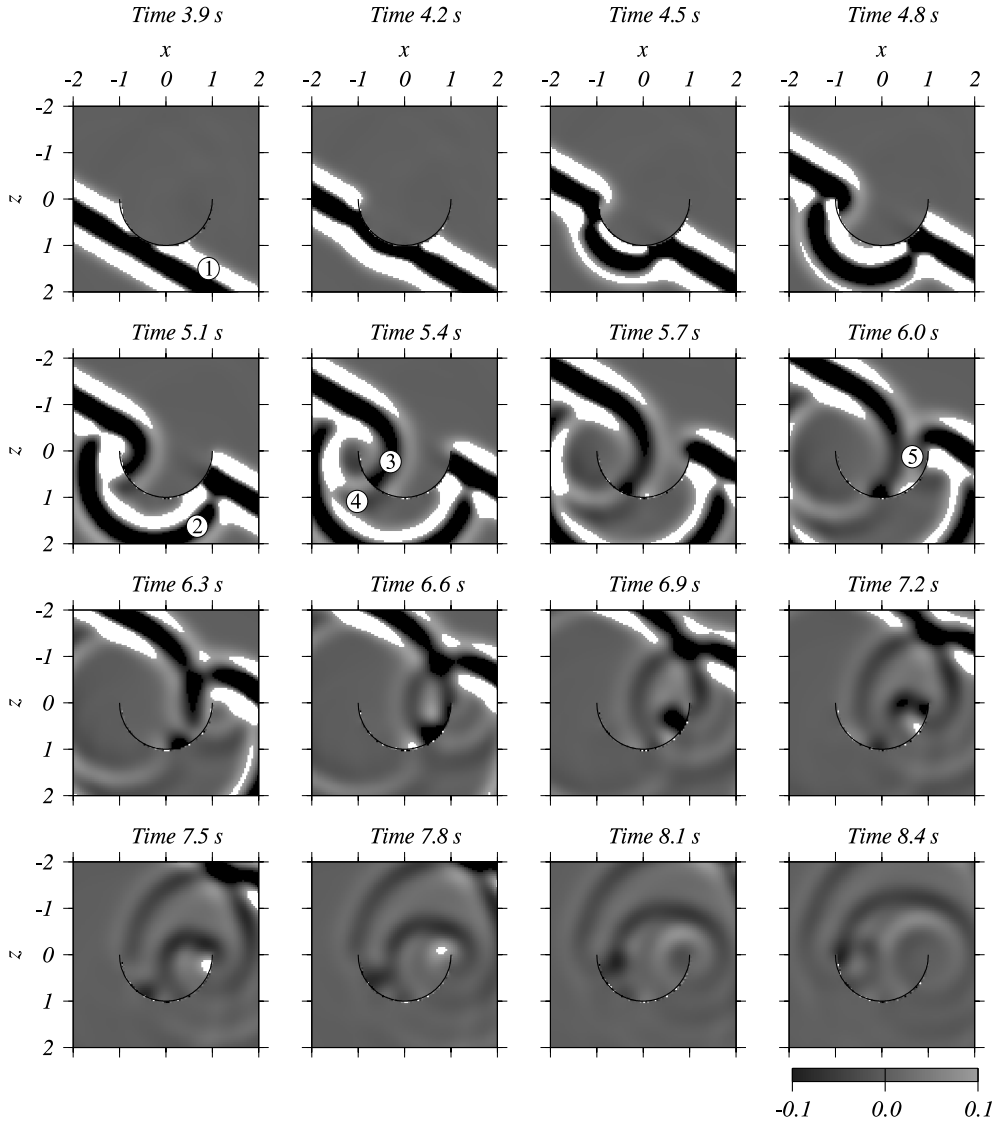

Figure 6. An *SH* plane wave with incidence angle $\gamma = 30^\circ$ (with respect to the z-axis) strikes a semi-circular crack with radius $r = 1$ and zero thickness. The incident time signal is a Ricker wavelet with characteristic period $t_p = 1.0$ s and $t_s = 5.0$ s. (1) Denotes the incident wavefield. (2) Corresponds to the reflected wave. (3) Is the diffracted wave generated at the left edge of the crack. (4) This is the diffracted wave generated at the left edge of the crack on the illuminated side, is the counterpart of (3). The diffracted wave generated at the left edge of the crack is labelled (5) Identifies the diffracted wave generated at the left edge of the crack. Due to the shape of the crack the amplitude of the diffracted field is generally higher in the shaded region.

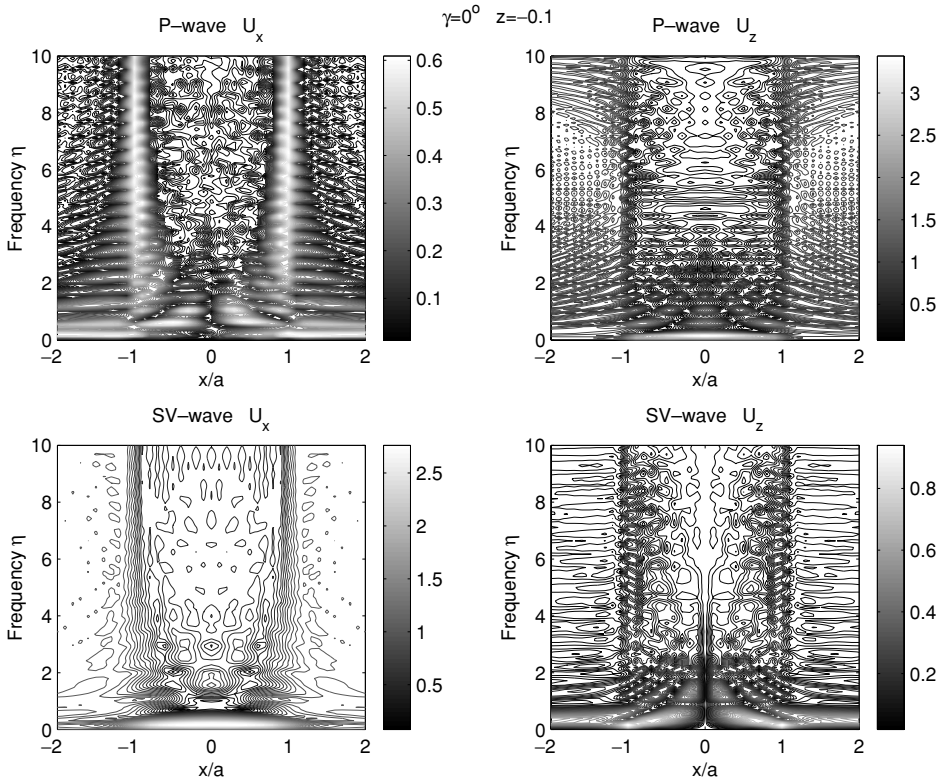

Figure 7. Contour maps of displacement amplitudes u_x and u_z given in eq. (11) for P (top) and SV incident waves (bottom). Incident angle $\gamma = 0^\circ$ (with respect to the z-axis). These (f–**x**) diagrams display the crack displacement amplitudes for 41 equally spaced receivers located along the interval $x \in [-2, 2]$ at $z = -0.1$ against the normalized frequency $\eta = \omega a/\pi\beta$. We use a Poisson's ratio of $\nu = 0.33$ and $\beta = 1$. We can see symmetry on the four (f–**x**) diagrams.

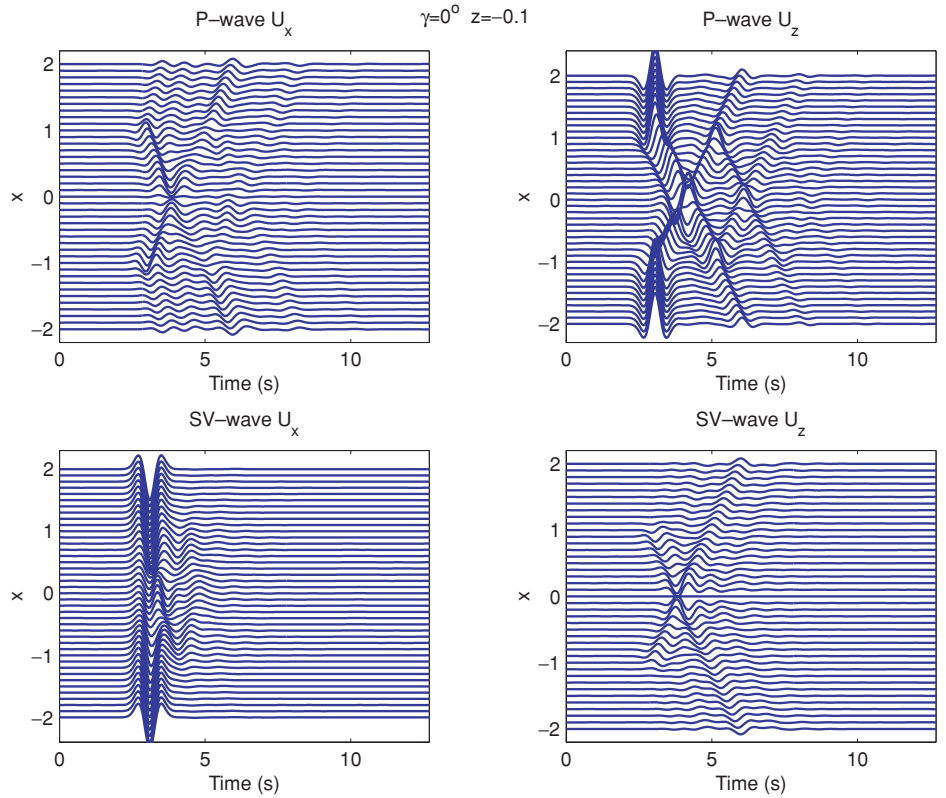

Figure 8. Synthetic seismograms are computed from frequency-domain results using a Fast Fourier Transform (FFT). The traces correspond to the total field for 41 equally spaced receivers located along the interval $x \in [-2, 2]$ at $z = -0.1$. The incident time signal is a Ricker wavelet with characteristic period $t_p = 1$ s. and $t_s = 3$ s. This case is for a Poisson's ratio of $\nu = 0.33$ and $\beta = 1$. Seismograms for both u_x and u_z displacements are included.

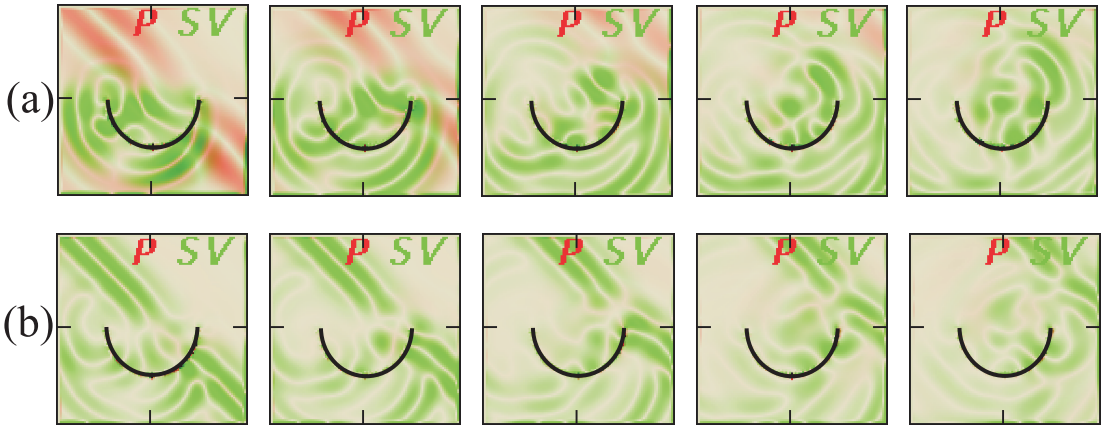

Figure 9. A *P*- and *SV* plane waves [(a) and (b), respectively], with incidence angle $\gamma = 45^\circ$ (with respect to the *z*-axis) strike a semi-circular crack with radius $r = 1$ and zero thickness. The incident time signal is a Ricker wavelet with characteristic period $t_p = 1.0$ s and $t_s = 5.0$ s. This case is for a Poisson's ratio of $\nu = 0.33$ and $\beta = 1$. A set of 101×101 equally spaced receivers are located on the square $[-2, 2] \times [-2, 2]$. We have computed the rotational and divergence fields to display the *P*- and *SV* waves (red and green respectively). Note that for both incidences scattering is stronger for *SV* waves than for *P* waves. The incident *P* wave quickly disappears and diffraction is mainly of *S* waves.

shown in Fig. 7. Both *P* and *SV* incident waves with $\gamma = 0^\circ$ are considered. We use a Poisson's ratio of $\nu = 0.33$ and $\beta = 1$. Symmetry is correctly preserved when a symmetric excitation is used.

Fig. 8 shows synthetic seismograms for 41 equally spaced receivers located at $z = -0.1$ with $x \in [-2, 2]$. The incident time signal is a Ricker wavelet with characteristic period $t_p = 1$ s. and $t_s = 3$ s. This case is for a Poisson's ratio of $\nu = 0.33$ and $\beta = 1$. We see *P*- wave incidence at the top and *SV* wave incidence at the bottom, u_x and u_z components are shown.

Fig. 9 shows the response of a crack excited by *P* and *SV* plane waves ((a) and (b) respectively), with incidence angle $\gamma = 45^\circ$ (with respect to the *z*-axis). The crack is semi-circular (as shown in Fig. 5) with radius $r = a = 1$ and zero thickness. The incident signal is a Ricker wavelet with characteristic period $t_p = 1.0$ s and $t_s = 5.0$ s. This case is for a Poisson's ratio of $\nu = 0.33$ and $\beta = 1$. A set of 101×101 equally spaced receivers are located on the square $[-2, 2] \times [-2, 2]$. We have computed the rotational and divergence fields to display the *P*- and *SV* waves (red and green respectively). Note that for both incidences scattering is stronger for *SV* waves than for *P* waves. The incident *P* wave quickly disappears and diffraction is mainly of *S* waves.

4 CONCLUSIONS

We have tested IBEM to solve scattering of *SH* waves by a zero-thickness crack. The method was tested against an analytical solution, for a canonical case, obtaining excellent agreements. By splitting the crack into two different domains, problems related to hyper-singularities have been overcome. The IBEM allows us to study media with arbitrary shaped cracks *SH* and *P–SV* wave scattering. More complex configurations of heterogeneities, fluid-filled cracks or cavities and 3-D cases will be presented in further publications using this technique. Computational costs increase with the frequency, this limits the resolution and is a serious constrain. However, parallel computing for methods in the frequency domain is much simpler than time domain computation based on domain decomposition. This is an advantage of the IBEM and it will help to study more realistic problems in the near future. Numerical results are encouraging but further work is needed to be able to deal with the inverse problem, that is, to determine the crack's shape, size and location from scattered wavefields.

ACKNOWLEDGMENTS

We would like to thank the keen comments from two anonymous reviewers that helped to improve the manuscript. This work has been partially supported by Instituto Mexicano del Petróleo under project D.00301, DGAPA-UNAM, México under grant IN121202 and Conacyt México under project NC-204.

REFERENCES

Achenbach, J.D., 1973. *Wave propagation in Elastic Solids*, North-Holland, Amsterdam.

Achenbach, J.D., Gautesen, A.K. & McMaken, H., 1982. *Ray methods for waves in elastic solids with applications to scattering by cracks,* Pitman, London.

Aki, K. & Richards, P.G., 1980. *Quantitative Seismology,* W.H. Freeman, San Francisco.

Aliabadi, M.H., 1997. Boundary elemeny formulations in fracture mechanics. *Appl. Mech. Rev.,* **50,** 83–96.

Ang, D.D. & Knopoff, L., 1964a. Diffraction of vector elastic waves by a finite crack, *Proc. Nat. Acad. Sci. USA,* **52,** 1075–1081.

Ang, D.D. & Knopoff, L., 1964b. Diffraction of vector elastic waves by a clamped finite strip, *Proc. Nat. Acad. Sci. USA,* **52,** 201–207.

Banerjee, P.K. & Butterfield, R., 1981. *Boundary Element Methods in Engineering Science,* McGraw Hill, London.

Bonnet, M., 1995. *Boundary integral equation methods for solids and fluids,* John Wiley & Sons, New York.

Coutant, O., 1989. Numerical study of the diffraction of elastic waves by fluid-filled cracks. *J. geophys. Res.,* **94,** 17 805–17 817.

Cruse, T.A., 1988. *Boundary element analysis in computational fracture mechanics,* Kluwer Academic Publishers, Boston USA.

Hevin, G., Abraham, O., Pedersen, H. & Campillo, M., 1998. Characterization of surface cracks with Rayleigh waves: a numerical model. *NDT International,* **31,** 289–297.

Hudson J.A., 1986. A higher order approximation to the wave propagation constants for cracked solid, *Geophys. J. R. astr. Soc,* **87,** 265–274.

Mal, A.K., 1970. Interaction of elastic waves with a Griffith crack. *Int. J. Engng. Sci.,* **8,** 763–776.

Ortiz-Alemán, C., Sánchez-Sesma, F.J., Rodríguez, J.L. & Luzón, F., 1998. Computing topographical 3-D site effects using a fast IBEM/Conjugate Gradient approach. *Bull. seis. Soc. Am.,* **88,** 393–399.

Pointer, T., Liu, E. & Hudson, J., 1998. Numerical modelling of seismic waves scattered by hydrofractures: application of the indirect boundary element method. *Geophys. J. Int.,* **135,** 289–303.

Prosper, D., 1998. Modeling and detection of delamination in laminated plates. *PhD thesis*, Massachusetts Institute of Technology.

Sánchez-Sesma, F.J. & Campillo, M., 1991. Diffraction of *P*, *SV* and Rayleigh waves by topographic features: a bounday integral formulation. *Bull. seis. Soc. Am.,* **81,** 2234–2253.

Sánchez-Sesma, F.J. & Iturrarán-Viveros, U., 2001. Scattering and diffraction of *SH* waves by a finite crack: an analytical solution. *Geophys. J. Int.,* **145,** 749–758.

van der Hijden, J.H.M.T. & Neerhof, F.L., 1984. Scattering of elastic waves by a plane crack of finite width. *Transactions of the ASME,* **51,** 646–651.

APPENDIX A: SUMMARY OF THE ANALYTICAL SOLUTION

Here we give a summary of the analytical solution used to test the IBEM for *SH* waves diffracted by a zero-thickness crack. For further details the reader is referred to Sánchez-Sesma & Iturrarán-Viveros (2001). The total field on the illuminated side of the crack is given by

$$v^{(t)^+} = 2v_0 e^{ikx\sin\gamma} - v^{(d)^-}, \tag{A1}$$

where the displacement $v^{(d)^-}$ on the shaded side is given by

$$v^{(d)^-} = v_0^{(d)^-} + \frac{v_1 Z - v_2}{1 - Z^2} s(r_1) F(\sqrt{2kr_1}) + \frac{v_2 Z - v_1}{1 - Z^2} s(r_2) F(\sqrt{2kr_2}), \tag{A2}$$

where

$$v_0^{(d)^-} = v_0 e^{-ika\sin\gamma} s(r_1)\, F\left(\sqrt{2kr_1}\sin\frac{\theta_0}{2}\right) + v_0 e^{ika\sin\gamma} s(r_2)\, F\left(\sqrt{2kr_2}\sin\frac{\theta_1}{2}\right), \tag{A3}$$

function v_1 is given by

$$v_1 = v_0 e^{-ika\sin\gamma} s(2a) F\left(\sqrt{4ka}\sin\frac{\theta_1}{2}\right), \tag{A4}$$

v_2 is given by

$$v_2 = v_0 e^{ika\sin\gamma} s(2a) F\left(\sqrt{4ka}\sin\frac{\theta_2}{2}\right), \tag{A5}$$

function Z is given by

$$Z = s(2a) F(\sqrt{4ka}), \tag{A6}$$

and the auxiliary function $s(r)$ is

$$s(r) = \frac{2}{\sqrt{\pi}} e^{ikr - i\frac{\pi}{4}}. \tag{A7}$$

Function F is a Fresnel integral given by

$$F(z) = \exp(-iz^2) \int_z^\infty \exp(i\tau^2)\, d\tau \tag{A8}$$

In addition we have that

$$v^{(d)^+} = -v^{(d)^-} \quad \text{and} \quad v^{(t)^-} = v^{(d)^-}. \tag{A9}$$